

Article

Digital Hydraulic Design for Low-Specific-Speed Propeller Runners with Fixed Blades

Youyu Liu ^{1,2} , Qijie Wang ^{1,2}, Dezhong Xu ^{1,2,*} and Qing Chen ³

¹ Key Laboratory of Advanced Perception and Intelligent Control of High-End Equipment, Ministry of Education, Wuhu 241000, China

² School of Mechanical Engineering, Anhui Polytechnic University, Wuhu 241000, China

³ EFORT Intelligent Equipment Co., Ltd., Wuhu 241009, China

* Correspondence: xdz@ahpu.edu.cn

Abstract: The operating point of a propeller hydropower station will deviate from the effective workspace while the discharge reduces excessively during dry seasons. It usually leads to a decrease in efficiency and even to being unable to work. To solve the above problem, a scheme named decreasing capacity to increase efficiency was presented in this article. A low-specific-speed propeller runner with fixed blades that has the same installing dimensions as the original one was redesigned and equipped in dry seasons. A positive circulation at the outlet of the blades bigger than in conventional runners is allowed. Some key technologies about hydraulic design for runner blades were researched, which include distribution of velocity circulation at the inlet and outlet of the runner, thickening of the epiphyseal line of an aerofoil, unfolding aerofoil being converted to a cylindrical section, etc. In the section on digital modeling for runner blades, aerofoils on the cylindrical sections at the rim and at the hub were constructed employing the trend extrapolation method. Moreover, a blade digital model was built at one time according to the aerofoils on all cylindrical sections by means of a successful redevelopment to UniGraphics, and it has perfect symmetry. A case presented indicates that the method of decreasing capacity to increase efficiency is feasible. Using the method, the turbine efficiency increased from less than 28.6% to 83.4% while the discharge decreased from $3.20 \text{ m}^3\text{s}^{-1}$ to $1.00 \text{ m}^3\text{s}^{-1}$, and then the hydropower unit was able to work properly.

Keywords: hydraulic turbines; propeller runners with fixed blades; low specific speed; trend extrapolation; decreasing capacity to increase efficiency



Citation: Liu, Y.; Wang, Q.; Xu, D.; Chen, Q. Digital Hydraulic Design for Low-Specific-Speed Propeller Runners with Fixed Blades. *Symmetry* **2022**, *14*, 2250. <https://doi.org/10.3390/sym14112250>

Academic Editors: Deming Lei and Jingcao Cai

Received: 26 September 2022

Accepted: 13 October 2022

Published: 26 October 2022

Publisher's Note: MDPI stays neutral with regard to jurisdictional claims in published maps and institutional affiliations.



Copyright: © 2022 by the authors. Licensee MDPI, Basel, Switzerland. This article is an open access article distributed under the terms and conditions of the Creative Commons Attribution (CC BY) license (<https://creativecommons.org/licenses/by/4.0/>).

1. Introduction

A propeller turbine is a kind of axial flow hydro-turbine in which the fixed blades have the advantages of large overflowing, high efficiency and good cavitation performance. Moreover, the processing cost of the unit is low. It is also convenient to be installed, operate and maintain. The propeller turbine is appropriate for a medium-mini size hydropower unit [1]. Currently, the standardization and serialization of medium-mini size hydropower units have been formulated, which have already formed one more complete system. In addition, several new components are currently being developed constantly. For example, Uchiyama et al. developed a micro-hydraulic turbine with excellent performance in the passage of foreign matter included in the water flow [2]. The runner has four blades, with a circular hollow around the rotating axis to pass foreign matter through the runner. Moreover, Ma et al. designed an inlet guide, vane and runner for developing a 2.5 kW hydraulic turbine. The efficiency and power of the turbine increased by 0.95% and 1.45%, respectively, compared to those of the reference model [3].

As for the development of propeller runners, at present, most scholars are absorbed in improving single capacity and increasing efficiency. For example, aiming at the problem of the insufficient output of the Huangtankou Hydropower Station, based on the existing conditions, a runner optimization design was implemented by CFD in reference [4], and

an appropriate turbine type was selected to realize the capacity expansion. The maximum output is increased by more than 10% compared with the original runner, and unit efficiency is improved significantly. In addition, Li Tao [5] studied the transformation of an axial flow turbine about capacity and corrosion in the Dujiangyan Shuangbo power station. Using an improved lifting model, the capacity of the transformed unit increases from 5000 kW to 6000 kW under the design condition, and its efficiency of it is 91.1%, which is 2.1% higher than the design one (89%).

The performance curves of propeller turbines are narrow [6], which means that it is more sensitive to discharge changes. As for most small and medium hydropower stations in many regions, the distribution of water resources in each season is highly uneven. Generally, the discharge is greatly reductive during dry seasons, and then the operating point is more likely to deviate from the effective workspace, which will usually lead to a decrease in efficiency and even to being unable to work. What had mentioned is a difficult problem in many hydropower stations. A feasible method to solve this problem is to reduce the unit capacity in exchange for raising its efficiency. Keeping the original full passage unchanged, only a new runner named low-specific-speed propeller runner with fixed blades is redesigned and manufactured to replace the original one. The implementation plan allows hydropower units that otherwise wouldn't be able to work to do so properly under the low-discharge conditions, which will increase the availability of water resources and equipment, and improve economic benefit greatly. Low-head or low-specific-speed propellers [7], and even low-specific-speed pumps [8], are also hot research topics at present.

With its rapid development of it, computer technology has been widely used in the research of the design and manufacture of runners. Computer-aided design can be applied to the hydraulic design of turbine runners and will raise their design efficiency and design accuracy greatly. For example, according to the Standard Modular Hydropower Technology proposed by the U.S. Department of Energy in 2017, Chen J provided a basic design methodology and some geometrical considerations on Digital hydraulic design. Additionally, he also presented some numerical simulation contents about several blade configurations, including stator blade inlet angle, runner blade solidity, and runner blade thickness, and how those geometrical configurations affect the overall performance and fluid behaviors [9]. Due to the actual flow at the rim and hub cannot meet the independence assumption among cylindrical layers, their aerofoils on the cylindrical sections cannot be designed by the hydraulic calculation method. Consequently, during the 3D modeling course for a runner blade, the aerofoils in the rim and hub can only be extended according to several aerofoils obtained by calculating. As for 3D modeling for a runner blade, many scholars are absorbed in surface reconstruction techniques. For instance, using a surface approach, the free-form shape of a 3D camber surface was defined by a multi-directional interpolation procedure, using the section approach, a Direct Profiling method was tested to fitting a hydrofoil section to the real one in reference [10]. The technique can be used to reverse and reconstruct an existing runner surface, however, is unable to extend it to the two sides keeping the original trend.

Trend extrapolation is a method for predicting society, economy, science and technology. Its fundamental assumption is that future is a continuous development along the past and present. Currently, trend extrapolation is mainly used for information research. For example, Meng, et al. used the household electricity consumption and population data of 30 provinces in China during 2001–2014, developed a hybrid trend extrapolation model to explore the driving factors of household electricity consumption growth in China and forecasted its future development trend before 2030 [11]. Friji, et al. proposed a generalized mechanistic model characterizing the COVID-19 pandemic evolution from a susceptible state to a discharged state. Once the model's parameters are estimated, forecasting results are derived, and uncertainty regions of the expected scenarios are provided [12]. According to the similarities between curve extension and information research, we studied several intelligent extension-models in Reference [13] by introducing trend extrapolation, with which

non-circular curves in planes can be extended intelligently for a short distance. However, the method and models are not available for spatial non-circular curves or surfaces.

In view of the difficult problem of the propeller, the turbine runs properly while the discharge reduces excessively during dry seasons; a modification plan of decreasing capacity to increase efficiency has been presented, and several key technical problems in hydraulic design have been solved in this article. In addition, a digital design method for runner blades has been developed by applying trend extrapolation to the extension of spatial non-circular curves and surfaces. In the end, the research achievement is applied to an instantiation; the validity of the theoretical analysis is proved.

2. Reasons and Solutions for Failure to Generate

2.1. Reasons for Failure to Generate

The inlet of a propeller runner has no impact, yet the outlet is along a normal direction under design conditions [14]. However, the design condition corresponds only to a certain head and discharge. But in actual operation, due to the changes in reservoir level and external load, head and discharge can frequently change, which will often make the propeller turbine off its optimum operating condition. The farther the operating condition from the design condition, the more efficiency declines.

Assuming the optimal operating condition of an original runner under high discharge to be “A”, while the operating condition unable to generate under low discharge to be “B”. The velocity triangles at the inlet and outlet of the airfoil are shown in Figure 1, where the velocity circulation at the outlet of the cylindrical surface is zero. The blade inlet angle will decrease from α'_1 to α''_1 when the guide vane opening decreases under low-discharge conditions, due to the velocity circulation at the outlet on the cylindrical section being zero, $v'_{2u} = 0$. The value of the absolute velocity at the inlet depends on H , hence is constant; the direction of it varies with the guide vane opening, namely $v''_1 = v'_1$. The value of a circular velocity depends on the generated frequency; hence, it is constant. Therefore, $u''_1 = u'_1 = u''_2 = u'_2$. According to the independence assumption among cylindrical layers [15], the value and direction of the meridional velocity at the outlet should be equal to that at the inlet, hence $v'_{2m} = v'_{1m}$, and $v''_{2m} = v''_{1m}$. The blade outlet angle of a propeller runner is unable to adjust, and then β'_2 remains constant, namely $\beta''_2 = \beta'_2$.

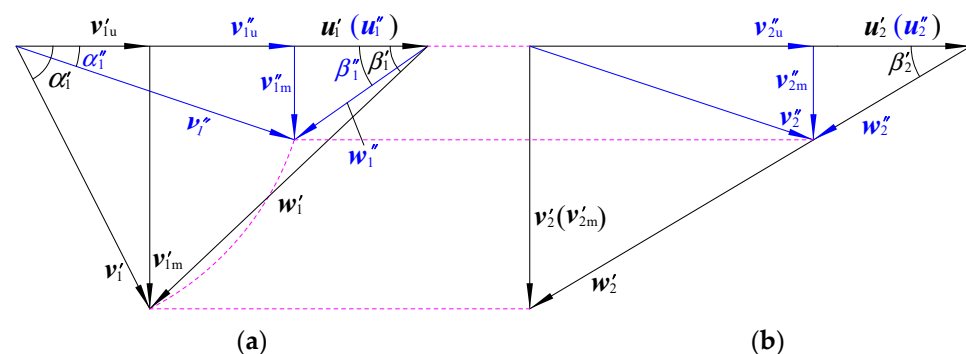


Figure 1. Velocity triangles at the inlet and outlet of the original runner: (a) Inlet, (b) Outlet.

As shown in Figure 1b, the value of v''_{2u} is too large, which means the Γ''_2 is too large. According to the fundamental equation $H''\eta_s''g = \omega''(\Gamma''_1 - \Gamma''_2)/2\pi$, $\Delta\Gamma''$ being too little will make a sharp drop in efficiency in the case that both H'' and ω'' are constant. The propeller turbine will be unable to work because of too little η_s'' if the discharge descends to a certain value. Moreover, v''_{2u} being too large does not favor to energy recovery for draft tubes [16], which can not only decrease efficiency but also reduce the running stability of units. As shown in Figure 1a, $\beta''_1 < \beta'_1$, so there is a great negative flow impact on the outlet under the condition “B”. Thus, the hydraulic loss is enormous [17] and the hydraulic efficiency of unit will reduce. For example, the optimal flow of GOE430 runner in a hydropower station is $3.20 \text{ m}^3\text{s}^{-1}$. When the discharge declines to $1.5 \text{ m}^3\text{s}^{-1}$, the velocity

circulation difference $\Delta\Gamma'' = 3.02 \text{ m}^3\text{s}^{-1}$. The η_s'' falls into 28.6%, and the units are unable to work completely.

2.2. Solutions for Failure to Generate

To solve the above problem, we present a scheme as follows. A low-specific-speed propeller runner with fixed blades, named new runner, that has the same installing dimensions with the original one is redesigned. The new runner and the original one are used interchangeably, corresponding to dry seasons and rainy seasons. As in the following, the unit can work properly under different seasons. On account of the original flow passage components remain unchanged, the reconstruction budget is the lowest.

As for the new runner, the parameters of the velocity triangles of the aerofoils on the same cylindrical section, against the original one, at the Inlet and Outlet under the condition “B” does not make any mark at the top-right corner. According to $Hg\eta_s = \omega(\Gamma_1 - \Gamma_2)/2\pi$ [18], H and ω being constant, if the velocity circulation difference of the new runner between inlet and outlet under the condition “B” reaches or approaches that of the original runner under the condition “A”, the efficiency of the new runner under the condition “B” reaches or approaches that of the original runner under the condition “A”. That is to say, $\Gamma_1 - \Gamma_2 = \Gamma'_1 - \Gamma'_2$. Consequently, $2\pi r v_{1u} - 2\pi r v_{2u} = 2\pi r v'_{1u} - 2\pi r v'_{2u}$. Due to $v'_{2u} = 0$ [15],

$$v_{2u} = v_{1u} - v'_{1u} \quad (1)$$

From the above analysis and Figure 2, some parameter relationships between the new runner under condition “B” and the original runner under condition “A” on the same cylindrical section are as follows.

$$v_1 = v''_1 = v'_1, \alpha_1 = \alpha''_1 < \alpha'_1; u''_1 = u'_1 = u'_1 = u''_2 = u'_2 = u'_2, \beta_2 < \beta'_2 = \beta''_2; v_{1m} = v_{2m} = v''_{1m} = v''_{2m}.$$

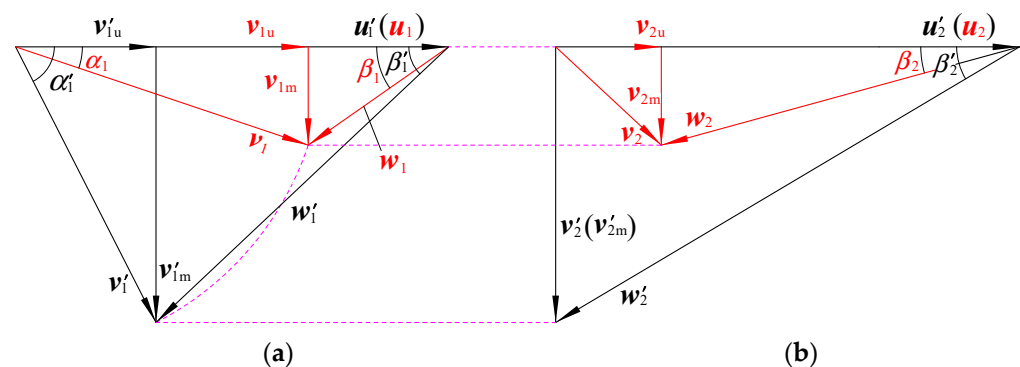


Figure 2. Velocity triangles at the inlet and outlet of new runner: (a) Inlet, (b) Outlet.

As shown in Figure 2b, v_{2u} is significantly less than v''_{2u} . Therefore, if the inlet angle and outlet angle of the new runner are approximately equal to the inflow angle and outflow angle, there is no or little positive impact at the entrance. Moreover, the velocity circulation of the outflow decreases greatly. In conclusion, the new runner can overcome the problem of the original runner under condition “B”.

3. Digital Hydraulic Design for Blades

As for the new runner, the average cascade solidity should be great for the unit discharge is rather small and the specific speed is very low [19]. Secondly, because of power output decreases, the load on the blade's declines compare to the original runners. Finally, as shown in Figure 1b, compare to the original runner, the relative velocity distribution in the vane passage of the new runner decreased greatly, but turbine setting, runner diameter and speed are the same with the original runners. As a result, the cavitation performances of the new runner depend exclusively on the designed aerofoils. Only if the aerofoils are reasonably well designed, can the cavitation performances be superior to the original

runner's [4]. In the process of design, the epiphyseal lines of the aerofoils are designed by singularity distribution method firstly, and then the epiphyseal lines are thickened on comparing the thickness variation of a certain excellent aerofoil that has the most suitable hydraulic parameters and similar specific speed against the new runner [20]. Several key technical problems in digital hydraulic design for runner blades are solved as follows.

3.1. Distribution of Velocity Circulation

There are three kinds of distribution of velocity circulation at the inlet and outlet of the runner [21]. One of them is that the velocity circulation at the outlet being zero lies in the cylindrical section (denoted by M-M) in the middle locations between the rim and hub, which is employed in this article. The distribution of the velocity circulation at the inlet and outlet of the new runner are shown in Figure 3 under condition "B". Considering the specialty of the design condition, a positive Γ_0 should be added to the initial distribution of velocity circulation at the outlet of the new runner. Consequently, the velocity circulation at the outlet on the M-M is Γ_0 .

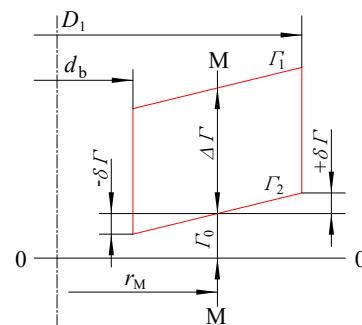


Figure 3. Distribution of velocity circulation at the inlet and outlet of the runner.

For the new runner, $n'_{110} = \frac{n'D_1}{\sqrt{H\eta'_s}}$ [21],

$$\omega' = \frac{2\pi n'}{60} = \frac{2\pi n'_{110} \sqrt{H\eta'_s}}{60D_1} \quad (2)$$

According to the fundamental equation of the turbine [21],

$$\Gamma'_1 - \Gamma'_2 = 2\pi r v'_{1u} - 2\pi r v'_{2u} = \frac{60gD_1 \sqrt{H\eta'_s}}{n'_{110}} \quad (3)$$

On the M-M, $\Gamma'_2 = 0$, then,

$$v'_{1u} = \frac{60gD_1 \sqrt{H\eta'_s}}{2\pi r_M n'_{110}} \quad (4)$$

From Figure 1a,

$$v_1 = v'_1 = \sqrt{v'^2_{1m} + v'^2_{1u}} = \sqrt{v'^2_z + v'^2_{1u}} \quad (5)$$

$$v_{1u} = \sqrt{v_1^2 - v'^2_{1m}} = \sqrt{v_1^2 - v_z^2} \quad (6)$$

From Equations (3)–(6), the velocity circulation of the new runner at the outlet on the M-M is as follows.

$$\Gamma_0 = 2\pi r_M v_{2u} = 2\pi r_M (v_{1u} - v'^2_{1u}) = 2\pi r_M \left(\sqrt{v'^2_z + v'^2_{1u}} - \frac{60gD_1 \sqrt{H\eta'_s}}{2\pi r_M n'_{110}} \right) \quad (7)$$

From the basic equation of the turbine,

$$\Delta\Gamma = \Gamma_1 - \Gamma_2 = \frac{2\pi H g \eta_s}{\omega} \quad (8)$$

According to the literature [21], the $\delta\Gamma$ shown in Figure 3 can be described as follows.

$$\delta\Gamma = 0.2(\Gamma_1 - \Gamma_2) = 0.2 \times \frac{2\pi H g \eta_s}{\omega} \quad (9)$$

If the velocity circulation at the outlet is regularly distributed in a straight line along the radius direction, its distribution is as follows.

$$\Gamma_2 = \Gamma_0 + \frac{4\delta\Gamma(r - r_M)}{D_1 - d_b} = 2\pi r_M \left(\sqrt{v_z'^2 + v_{1u}'^2 - v_z^2} - \frac{60gD_1\sqrt{H\eta_s'}}{2\pi r_M n_{110}'} \right) + \frac{1.6\pi H g \eta_s (r - r_M)}{(D_1 - d_b)\omega} \quad (10)$$

From Equations (8) and (10), the distribution of the velocity circulation at the inlet along the radius direction is as follows.

$$\Gamma_1 = 2\pi r_M \left(\sqrt{v_z'^2 + v_{1u}'^2 - v_z^2} - \frac{60gD_1\sqrt{H\eta_s'}}{2\pi r_M n_{110}'} \right) + \frac{1.6\pi H g \eta_s (r - r_M)}{(D_1 - d_b)\omega} + \frac{2\pi H g \eta_s}{\omega} \quad (11)$$

3.2. Thickening of Epiphyseal Line of Aerofoil

Several discrete points (11 points in this article) on every epiphyseal line of an aerofoil in stream surface can be calculated during the hydraulic calculation of the runner blade. A continuous epiphyseal line of aerofoil can be fitted according to the above discrete points, which can be thickened to an aerofoil with a certain thickness. GOE430 [20] shown in Figure 4 is an aerofoil to thicken accordingly in this article. The position of every discrete point calculated on the epiphyseal line may not coincide with that of the discrete point selected (17 points in literatures [20]). Consequently, the epiphyseal line of aerofoil must be interpolated into 17 points from the 11 points by calculating it according to the value before they are thickened. Those points are signed, respectively, from the outlet to the inlet. There are several interpolation methods, one of which is B-Spline interpolation. It enables the fit curves interpolated to pass all the date points. In addition, the first and second derivatives in nodes are continuous and smooth, and have a good convergence [22]. The b-Spline interpolation method is applied in this article. After the 17 points are interpolated, the thickened value y_B (marked as y_i^B) and y_H (marked as y_i^H) corresponding to the points can be calculated respectively.

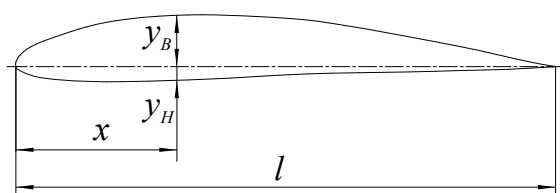


Figure 4. GOE430 aerofoil.

As shown in Figure 5, G_i and G_{i-1} ($i = 1, 2, \dots, 20$) are the two adjacent points obtained from interpolating. Obviously, the relative curvature of the blade aerofoil is minor, and the epiphyseal line $\overline{G_i G_{i-1}}$ is very short. Therefore, $\overline{G_i G_{i-1}}$ can be replaced by a line segment $\overline{G_i G_{i-1}}$. A point on the epiphyseal line is interpolated along its normal direction. That is to say, $\overline{H_i B_i}$ that is a line of the two points H_i and B_i on the front and the back of the aerofoil thickened is perpendicular to $\overline{G_i G_{i-1}}$.

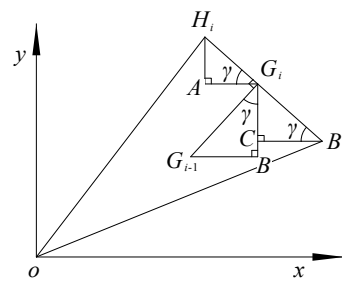


Figure 5. Thickening method for aerofoil.

As shown in Figure 5, the coordinates value of G_i , G_{i-1} , H_i , B_i are (x_i^G, y_i^G) , (x_{i-1}^G, y_{i-1}^G) , (x_i^H, y_i^H) , (x_i^B, y_i^B) respectively. From the right triangle AG_iH_i (marked as $Rt\Delta AG_iH_i$) in Figure 5, we can see: $\tan \Gamma = \frac{y_i^H - y_i^G}{x_i^G - x_i^H}$; from $Rt\Delta BG_iG_{i-1}$, $\tan \Gamma = \frac{x_i^G - x_{i-1}^G}{y_i^G - y_{i-1}^G}$; from $Rt\Delta CB_iG_i$, $\tan \Gamma = \frac{y_i^G - y_i^B}{x_i^B - x_i^G}$.

Due to $|H_iG_i| = y_{H_i}$ and $|B_iG_i| = y_{B_i}$, the following two equations can be obtained in $Rt\Delta AG_iH_i$ and $Rt\Delta CB_iG_i$ according to Pythagoras theorem with the above analysis.

$$\left. \begin{aligned} \frac{y_i^H - y_i^G}{x_i^G - x_i^H} &= \frac{x_i^G - x_{i-1}^G}{y_i^G - y_{i-1}^G} \\ (x_i^G - x_i^H)^2 + (y_i^H - y_i^G)^2 &= (y_i^H)^2 \end{aligned} \right\} \quad (12)$$

$$\left. \begin{aligned} \frac{y_i^G - y_i^B}{x_i^B - x_i^G} &= \frac{x_i^G - x_{i-1}^G}{y_i^G - y_{i-1}^G} \\ (x_i^G - x_i^H)^2 + (x_i^H - x_i^G)^2 &= (y_i^B)^2 \end{aligned} \right\} \quad (13)$$

The first point on the epiphyseal line of the aerofoil is not necessarily thickened because it is on the aerofoil surface [21]. The coordinate values (x_i^H, y_i^H) and (x_i^B, y_i^B) ($i = 2, 3, \dots, 17$) of the points H_i and B_i can be determined by Equations (12) and (13). Therefore, the coordinate values of 33 points on the aerofoil surface have been determined. A smooth curve can be fitted from these points by using B-Spline. Thus, an unfolded aerofoil with a certain thickness can be obtained.

3.3. Unfolding Aerofoil Converted to Cylindrical Section

The unfolding aerofoil should be converted to the corresponding cylindrical section in 3D solid modeling. According to the rotation-axis position determinacy [21], a line connecting all rotation axes of the aerofoil is perpendicular to the runner axis. Likewise, a line connecting all outlets of the aerofoil is also perpendicular to the runner axis. As shown in Figure 6, as for the airfoil i ($i = 1, 2, \dots, 5$), the rotation axis ($o_1'' o_i''$) of it is perpendicular to the runner axis, and intersect in the point o with it. The outlet ($A_1'' A_i''$) is also perpendicular to the runner axis, and intersect in the point o_A with it. It is obvious that all the rotation axes lie on $o_1'' o_i''$ and outlets on $A_1'' A_i''$. The radius of the aerofoil i on cylindrical section is r_i . As shown in Figure 6, $x_i'' y_i'' z_i''$ is a coordinate system for hydraulic calculation; moreover, its origin lies in the outlet. On the other hand, each coordinate axis of $x' y' z'$ is parallel to that of $x_i'' y_i'' z_i''$. z' -axis is coincident with the runner axis. In addition, its origin lies on the intersection of z' -axis and $o_1'' o_i''$. The coordinate values of a discrete point P_i'' on the aerofoil can be transformed into those in $x' y' z'$ using affine transformation [23]. See Equation (14), in which $(x_{o'}'', y_{o'}'', z_{o'}'')$ are the coordinate values of o' in $x_i'' y_i'' z_i''$.

$$\begin{bmatrix} x_i' \\ y_i' \\ z_i' \end{bmatrix} = \begin{bmatrix} x_i'' \\ y_i'' \\ z_i'' \end{bmatrix} - \begin{bmatrix} x_{o'}'' \\ y_{o'}'' \\ z_{o'}'' \end{bmatrix} \quad (14)$$

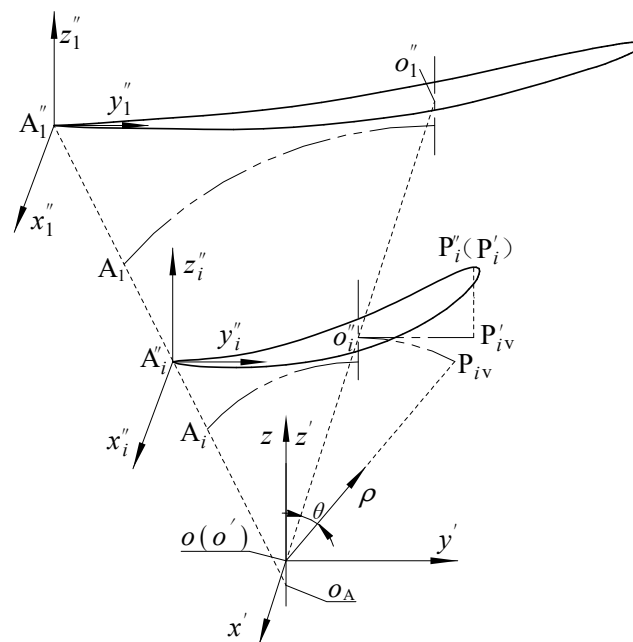


Figure 6. Discrete points on unfolding aerofoil being converted to cylindrical section.

The $z\rho\theta$ is a cylindrical coordinate system, its z -axis is coincident with the z' -axis of the $x'y'z'$, and its polar axis is just the rotation axis of the runner. As for the airfoil i , $|oo_i''| = r_i$. P_{iv}'' is a point that $P_i''(P_i')$ is projected onto the y' -axis. According to the relations between real 3D aerofoil and unfolding one, $|o_i'' P_{iv}''|$ equals to the arc length of $\overline{o_i'' P_{iv}''}$. As a result, the coordinate value of $P_i''(P_i')$ that is converted to the cylindrical section in $z\rho\theta$ is shown in Equation (15). According to the conversion relationship between the cylindrical coordinate system and spatial Cartesian coordinate system, the coordinate value of $P_i''(P_i')$ in the cylindrical section in $x'y'z'$ is shown in Equation (16).

$$\begin{bmatrix} \rho_i \\ \theta_i \\ z_i \end{bmatrix} = \begin{bmatrix} 1 & 0 & 0 \\ 0 & -1/r_i & 0 \\ 0 & 0 & 1 \end{bmatrix} \begin{bmatrix} r_i \\ y_i' \\ z_i' \end{bmatrix} \quad (15)$$

$$\begin{bmatrix} x_i \\ y_i \\ z_i \end{bmatrix} = \mathbf{E} \begin{bmatrix} \rho_i \cos \theta_i \\ \rho_i \sin \theta_i \\ y_i \end{bmatrix} \quad (16)$$

4. Digital Hydraulic Design for Runner Blades

Aerofoils on cylindrical section obtained by a hydraulic design for the runner blade are finite, usually are five in the middle of the blade, as shown in Figure 7. The aerofoils on cylindrical sections are saved to an EXCEL file in the form of point coordinates. The EXCEL file is converted into a “.csv” format ready for import into Imageware [24]. A bitmap of the blade can be obtained, and then saved it as a “.igs” format, put it into UniGraphics. Finally, the points of aerofoil on cylindrical section are grouped in proper order and form a close curve by the “Spline Fitting” [25].

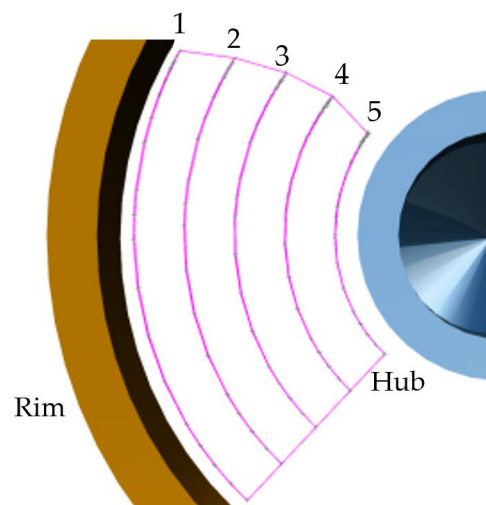


Figure 7. Aerofoils on Cylindrical Sections.

Because the actual flow of the turbine in the rim and hub cannot meet the independence assumption among cylindrical layer. Therefore, the aerofoil of the cylindrical section is difficult to be obtained through hydraulic design and calculation. It brings great difficulties for the 3D model of runner blades. With respect to this problem, two possible solutions are provided, and then their performance characteristics are analyzed and compared.

4.1. Projection

The curve of the nearest aerofoil 1 on the cylindrical section to the rim is projected onto the rim cylinder, which is taken as an approximate section curve of the aerofoil on the rim cylinder. Similarly, the curve of the nearest aerofoil 5 on the cylindrical section to the hub is projected onto the hub cylinder, which is taken as an approximate section curve of the aerofoil on the hub cylinder. A 3D model of the runner blade can be built according to the seven section curves by means of “Through Curves” in UniGraphics. The single blade model is shown in Figure 8a. The integrated runner digital model is shown in Figure 8b. In projection method, the aerofoil on cylindrical section at the rim or hub is formed by projecting the nearest aerofoil to the rim or hub cylinder. That is to say, the projected aerofoil is zoomed in or out based on the runner axes. As shown in Figure 8a, the positions A and B on the inlet of the runner are not in accordance with the trend of its middle part obtained by hydraulic calculation. Therefore, it is difficult to conform to the hydrodynamic rule, which will lead to a decrease in hydraulic efficiency.

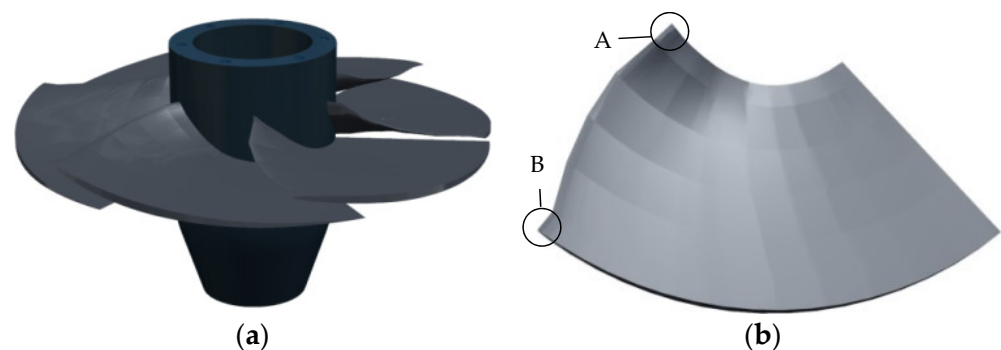


Figure 8. Runner digital model via projection: (a) single blade model, (b) runner digital model.

4.2. Trend Extrapolation

Three kinds of intelligent extension-models [13] such as multinomial extension-model, exponential extension-model and Gompertz extension-model had been built by introducing trend extrapolation, which can be selected and used reasonably according to the feature

points of curves. Almost all non-circular curves in plane can be extended intelligently. The study also found that a curve extended near the starting point is proving well by comparison with the theoretical curve. The closer the distance from the starting point, the higher the accuracy is. 33 homonymous points on the five aerofoil curves gained by hydraulic calculation need to be fitted using a curve. It is obvious that the fitting curve is a spatial curve. Therefore, the extension technology for planar curves based on trend extrapolation in reference [13] is not immediately available.

4.2.1. Extending Spatial Curve

33 homonymous points on the five aerofoil curves are marked as P_i^k , where k equals to 1, 2, ..., 5; i equals to 1, 2, ..., 33. As shown in Figure 9, S is a curve fitted by the homonymous points i on the five aerofoil curves. Its expressions are as follows.

$$\begin{aligned} F(x_i, y_i, z_i) &= 0 \\ G(x_i, y_i, z_i) &= 0 \end{aligned} \quad (17)$$

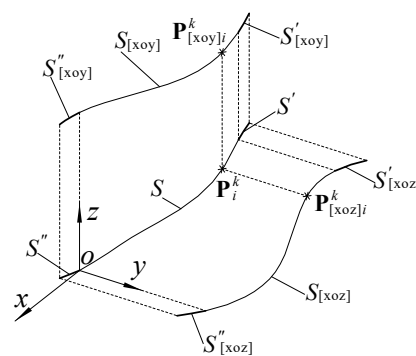


Figure 9. Extending spatial curve using trend extrapolation.

The P_i^k in the curve S are projected onto the plane xoy , the projected points of which are marked as $P_{[xoy]i}^k$; similarly, the P_i^k are projected onto the plane xoz , the projected points of which are marked as $P_{[xoz]i}^k$. As shown in Figure 9, the projected points $P_{[xoy]i}^k$ can be fitted into a plane curve $S_{[xoy]}$, see in Equation (18); likewise, $P_{[xoz]i}^k$ can be fitted into $S_{[xoz]}$, see in Equation (19).

$$\begin{cases} S_{[xoy]}(x_i, y_i) = 0 \\ z_i = z_0 \end{cases} \quad (18)$$

$$\begin{cases} S_{[xoz]}(x_i, z_i) = 0 \\ y_i = y_0 \end{cases} \quad (19)$$

As shown in Figure 9, the radiuses of the cylinders from Section 1 to Section 5 are decreasing at an arithmetic progression rate. That is to say, $r_{i+1} - r_i$ are all constant. On the other hand, the difference of that between the rim and Section 1 is $(r_{i+1} - r_i)/2$, the same as between Section 5 and the hub. As for the plane curves $S_{[xoy]}$ and $S_{[xoz]}$, due to the parts of them to be extended are approximately 10% of the length of the original curves, they only need to be extended for a short distance. According to the literature [13], the extension technology for plane curves based on trend extrapolation can be adopted.

As shown in Figure 9, the curves $S_{[xoy]}$ and $S_{[xoz]}$ can be extended respectively in rim direction using the extension technology for plane curves based on trend extrapolation in literature [13]. Thus, the plane curves $S'_{[xoy]}$ and $S'_{[xoz]}$ can be obtained, and their expressions are shown in Equations (20) and (21).

$$\begin{cases} S'_{[xoy]}(x_j, y_j) = 0 \\ z_j = z_0 \end{cases} \quad (20)$$

$$\begin{cases} S'_{[xoz]}(x_j, \hat{z}_j) = 0 \\ y_j = y_0 \end{cases} \quad (21)$$

Taking $S'_{[xoy]}$ and $S'_{[xoz]}$ as two generatrices, two cylindrical surfaces can be formed by them being stretched along the z -axis and the y -axis respectively. Eventually, they are crossing on the curve S' . Their expressions are shown in Equation (22).

$$\begin{cases} S'_{[xoy]}(x_j, \hat{y}_j) = 0 \\ S'_{[xoz]}(x_j, \hat{z}_j) = 0 \end{cases} \quad (22)$$

In the same way, the curves $S_{[xoy]}$ and $S_{[xoz]}$ can be extended respectively in hub direction, and then the plane curves $S''_{[xoy]}$ and $S''_{[xoz]}$ can be obtained. Taking $S''_{[xoy]}$ and $S''_{[xoz]}$ as two generatrix, two cylindrical surfaces can also be formed by them being stretched along the z -axis and the y -axis respectively. They are crossing on the curve S'' . The curves S' and S'' are the intelligent extension parts, respectively, of the spatial curve S along the rim and the hub direction. The intersections of the curve S' with the rim cylinder are marked as P_i^6 ; the intersections of the curve S'' with the hub cylinder are marked as P_i^0 .

4.2.2. Digital Modeling for Runner

A hydraulic design program for runner blades has been developed by using MATLAB, in which the 33 discrete points on each of the five aerofoil curves gained by hydraulic calculation have been fitted into a closed curve by using a B-Spline [22]. By means of the above method of extending spatial curve using trend extrapolation, the homonymous points P_i^6 and P_i^0 on the aerofoils on the rim and hub separately can be obtained. Similarly, those points can be fitted into hub aerofoil and rim one separately by using B-Spline. The top view of the extending curves of aerofoils on the cylindrical section is shown in Figure 10a; the spatial diagram of the extending curves of aerofoils on the cylindrical section is shown in Figure 10b. The same as projection method, a 3D model of the runner blade can also be built according to the seven section curves by means of “Through Curves” in UniGraphics. The single-blade model is shown in Figure 11a. The integrated runner digital model is shown in Figure 11b. Unlike Figure 8, the aerofoils on the inlet of the runner are accord with the trend of its middle part. Therefore, there is a high hydraulic efficiency for the runner.

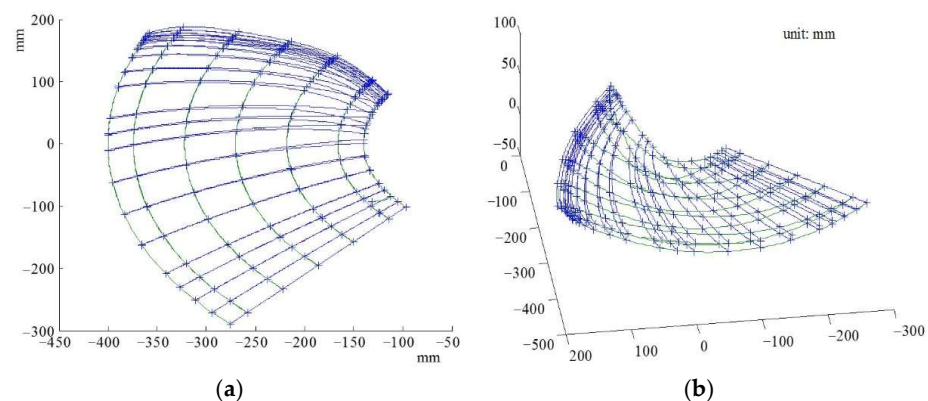


Figure 10. Extending curves of aerofoils on cylindrical section: (a) top view, (b) spatial diagram.

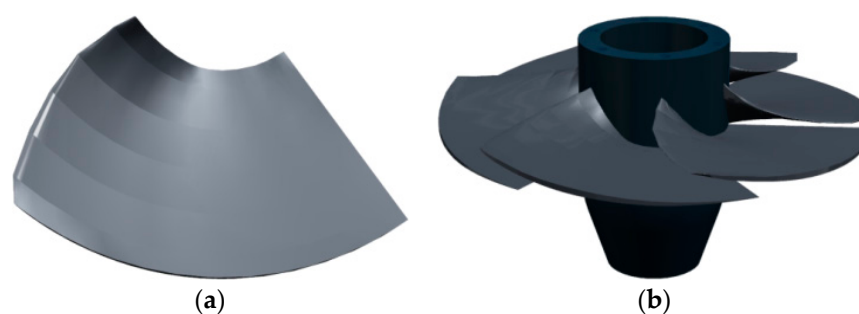


Figure 11. Runner digital model via trend extrapolation: (a) Single Blade Model, (b) Runner Digital Mode.

By means of the manual modeling method “Through Curves” in UNIGRAPHICS, two aerofoil curves are selected each time to generate part of the aerofoil surface, which is partial and fractional. Thus, the surface is discontinuous in junction. As shown in Figures 8 and 11, the surface obtained is not smooth, which will necessarily lead to a decrease in hydraulic efficiency. In order to make the blade surface became smooth and continuous, an optimization program was developed and integrated into UNIGRAPHICS using Visual C++ in this article. The seven aerofoil curves can be imported into the program running in the NX Open Grip environment at one time, and then those curves are picked up in turn using sphere.grx to fit into a B-surface at once [22]. The single blade model optimized is shown in Figure 12a. The integrated runner digital model optimized is shown in Figure 12b. Compared with the runner model shown in Figure 11, the blade surface of that shown in Figure 12 is continuous and smooth, and has better flow-field stability and higher hydraulic efficiency.

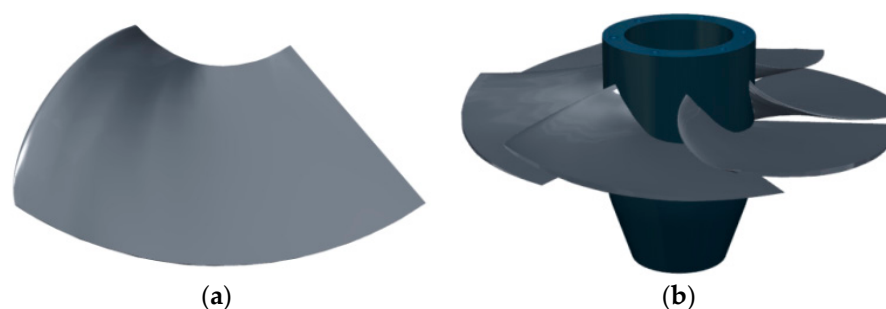


Figure 12. Runner Digital Model Optimized: (a) Single Blade Model, (b) Runner Digital Model.

5. Case

The basic parameters of runner GOE430 in a hydropower station are shown in Table 1. Rated discharge during rainy seasons is $3.20 \text{ m}^3\text{s}^{-1}$. While the discharge decreased to $1.00 \text{ m}^3\text{s}^{-1}$ during dry seasons, the hydropower unit is unable to work.

Table 1. Operating condition parameters.

Parameters	H	n	Q	D_1	d_b	η_s	η
Units	m	$\text{r}\cdot\text{min}^{-1}$	m^3s^{-1}	mm	/	/	/
Value	13.50	750	1.00	800	0.35	90%	80%

A new runner used in dry seasons has been designed according to the plan of decreasing capacity to increase efficiency, in which part of the intermediate and final results are as follows: $n_{110} = 172.1 \text{ r/min}$; $Q_{110} = 0.4483 \text{ m}^3\text{s}^{-1}$; $n_s = 322.6 \text{ m}\cdot\text{kW}$; incremental velocity circulation $\Gamma_0 = 1.46 \text{ m}^2\text{s}^{-1}$; $(l/t)_{pj} = 1.5$; $Z = 6$. Based on GOE430, a new runner that has been designed and manufactured is shown in Figure 13, which has been put into operation. By running in experiment test and practical work, $\eta = 83.4\%$, it can fulfill power properly.



Figure 13. New runner designed and manufactured.

6. Conclusions

The reason for the unit being unable to generate is that the velocity circulation at the outlet of the original runner is too large under low-discharge conditions during dry seasons, and then its hydraulic efficiency would reduce sharply. To solve the problem, a low-specific-speed propeller runner with fixed blades has been redesigned and equipped in dry seasons according to the scheme of decreasing capacity to increase efficiency. The new runner has the same installing dimensions, the same runner type, and some parameters with the original one. However, a positive circulation at the outlet of the blades bigger than in a conventional runner is allowed. Moreover, the new runner has bigger cascade solidity, a greater number of blades, and then has better cavitation characteristics. Computer-aided design technologies are employed in hydraulic design. Such methods as “thickening of epiphyseal line of aerofoil” and “unfolding aerofoil being converted to cylindrical section” have been researched and worked out. Hence it becomes possible to reduce R & D cycle, and improve design efficiency greatly. The runner digital model provides a foundation for CFD analysis and NC manufacturing. A method to establish the aerofoils on the cylindrical sections at the rim and hub has been provided. Employing trend extrapolation in this article, a spatial curve can be extended successfully. Thus, the aerofoils on the cylindrical sections can also be extended along the rim and hub direction according to their tendency. Comparing to projection method, this method can gain a runner blade with its surface being more in line with the trend of the middle part, and being more accord with fluid dynamics. Thus, the hydraulic efficiency is higher. The blade curves have been established through secondary development of UNIGRAPHICS with Visual C++ according to the aerofoils on the cylindrical sections, and picked up in turn to fit into a B-surface at once. Comparing to “Through Curves”, the blade surface obtained is continuous and smooth, and has better flow-field stability and higher hydraulic efficiency. A new runner in the case has been successfully applied in a hydropower station. The result shows that the technical route is reasonable and scheme is rational and feasible. Using the method, the turbine efficiency increased from less than 28.6% to 83.4% while the discharge decreased from $3.20 \text{ m}^3\text{s}^{-1}$ to $1.00 \text{ m}^3\text{s}^{-1}$. The redevelopment came to a complete success.

Author Contributions: Conceptualization, Y.L. and D.X.; methodology, D.X. and Y.L.; software, D.X.; validation, Q.C., D.X. and Y.L.; formal analysis, Q.W.; investigation, Q.C.; resources, Q.C.; data curation, D.X.; writing—original draft preparation, Q.W.; writing—review and editing, Y.L.; visualization, Q.C.; supervision, D.X.; project administration, Y.L.; funding acquisition, Y.L. All authors have read and agreed to the published version of the manuscript.

Funding: Supported in part by Special Fund for Collaborative Innovation of Anhui Polytechnic University & Jiujiang District under Grant No. 2021CYXTB3, by Natural Science Research Project of Higher Education of Anhui Province of China under Grant No. KJ2020A0357, and by Natural Science Research Project of Higher Education of Anhui Province of China under Grant No. YJS20210446.

Institutional Review Board Statement: Not applicable.

Informed Consent Statement: Not applicable.

Data Availability Statement: Not applicable.

Conflicts of Interest: The authors declare no conflict of interest.

Nomenclature

α	inlet angle of blade (rad)
β	outlet angle of blade (rad)
Γ	angle (rad)
v	flow velocity (ms^{-1})
u	circumferential velocity (ms^{-1})
H	head (m)
Γ	velocity circulation (m^2s^{-1})
η_s	hydraulic efficiency
η	turbine efficiency
ω	angular velocity (rads^{-1})
r	radius (m)
r_M	radius of M-M cylindrical section
n	speed of revolution (r min^{-1})
n_{110}	optimum unit speed ($\text{r} \cdot \text{min}^{-1}$)
Q	discharge (m^3s^{-1})
Q_{110}	optimum unit discharge (m^3s^{-1})
n_s	specific speed ($\text{m} \cdot \text{kW}$)
$(l/t)_{pj}$	average cascade solidity
Z	number of blades
D_1	nominal Diameter (mm)
d_b	hub Ratio
\mathbf{E}	identity matrix
x_j	x -coordinate of the expansion-point j
\hat{y}_j	y -coordinate of the expansion-point j extended
\hat{z}_j	z -coordinate of the expansion-point j extended
Subscripts	
1	inlet
2	outlet
u	circumferential direction
m	meridional direction
z	direction of shaft
i	serial number of points.
Superscripts	
'	parameters of the original runner when working under the condition "A"
"	parameters of the original runner when working under the condition "B"
k	serial number of aerofoils.

References

- Wei, Y.F.; Ma, Y.D. Research and Improvement on Runner Structure Optimization of Large Axial Flow Hydroturbine with Movable Blade. *Hongshui River* **2019**, *38*, 84–89. (In Chinese)
- Uchiyama, T.; Honda, S.; Degawa, T. Development of a propeller-type hollow micro-hydraulic turbine with excellent performance in passing foreign matter. *Renew. Energy* **2018**, *126*, 545–551. [\[CrossRef\]](#)
- Ma, S.B.; Kim, S.; Choi, Y.S.; Cha, D.A.; Kim, J.H. Development of 2.5 kW Class Propeller Type Micro Hydraulic Turbine. *Trans. Korean Hydrog. New Energy Soc.* **2020**, *31*, 314–321. [\[CrossRef\]](#)
- Zhu, D.J.; Wang, J.X. Research on Water Wing Reduction of Middle Pier of Large Slope Compact Overflow Dam. *Water Resour. Power* **2021**, *39*, 172–175. (In Chinese)
- Li, T. Retrofit and Design of Increasing Capacity and Cavitation Resistance of Kaplan Turbine Runner Based on CFD. Master's Thesis, Xihua University, Chengdu, China, 2013.
- Kim, B.K. Optimization of Micro Hydro Propeller Turbine blade using NSGA-II. *J. Fluid Mach.* **2014**, *17*, 19–29. [\[CrossRef\]](#)
- Barsi, D.; Ubaldi, M.; Zunino, P.; Fink, R. Optimized Design of a Novel Hydraulic Propeller Turbine for Low Heads. *Designs* **2021**, *5*, 20. [\[CrossRef\]](#)
- Chabannes, L.; Ștefan, D.; Rudolf, P. Effect of Splitter Blades on Performances of a Very Low Specific Speed Pump. *Energies* **2021**, *14*, 3785. [\[CrossRef\]](#)

9. Chen, J.B.; Engeda, A. Standard module hydraulic technology: A novel geometrical design methodology and analysis for a low-head hydraulic turbine system, part II: Turbine stator-blade and runner-blade geometry, and off-design considerations. *Energy* **2021**, *214*, 118982. [CrossRef]
10. Cerriteo, A.; Delgado, G.; Galván, S.; Dominguez, F.; Ramírez, R. Reconstruction of the Francis 99 main runner blade using a hybrid parametric approach. *IOP Conf. Ser. Earth Environ. Sci.* **2021**, *774*, 012074. [CrossRef]
11. Meng, M.; Wang, L.X.; Shang, W. Decomposition and forecasting analysis of China's household electricity consumption using three-dimensional decomposition and hybrid trend extrapolation models. *Energy* **2018**, *165*, 143–152. [CrossRef]
12. Friji, H.; Hamadi, R.; Ghazzai, H.; Besbes, H.; Massoud, Y. A Generalized Mechanistic Model for Assessing and Forecasting the Spread of the COVID-19 Pandemic. *IEEE Access* **2021**, *9*, 13266–13285. [CrossRef] [PubMed]
13. Yang, G.T.; Liu, Y.Y. Intelligent extension models andir applications for non-circular curves based on trend extrapolation. *Comput. Eng. Appl.* **2014**, *50*, 46–50. (In Chinese) [CrossRef]
14. Aeschlimann, V.; Beaulieu, S.; Houde, S.; Ciocan, G.D.; Deschenes, C. Inter-blade flow analysis of a propeller turbine runner using stereoscopic PIV. *Eur. J. Mech. B-Fluids* **2013**, *50*, 121–128. [CrossRef]
15. Waqas, M.; Ahmad, N. Computation of Stress Distribution in Hydraulic Horizontal Propeller Turbine Runner Based on Fluid-Structure Interaction Analysis. *Arab. J. Sci. Eng.* **2020**, *45*, 9325–9337. [CrossRef]
16. Karadi, U.; Bergant, A.; Starinac, D.; Boovi, B. Water Hammer Investigation of the Shut-Down of a High-Head Hydropower Plant at Very High Reynolds Number Flows. *Stroj. Vestn.-J. Mech. Eng.* **2019**, *65*, 430–440. [CrossRef]
17. Zhu, B.S.; Tan, L.; Wang, X.H.; Ma, Z. Investigation on Flow Characteristics of Pump-Turbine Runners with Large Blade Lean. *J. Fluids Eng.-Trans. Asme* **2018**, *140*, 031101. [CrossRef]
18. Singh, P.; Nestmann, F. Experimental investigation of the influence of blade height and blade number on the performance of low head axial flow turbines. *Renew. Energy* **2011**, *36*, 272–281. [CrossRef]
19. Brasil, A.C.P.; Mendes, R.C.F.; Wirrig, T.; Noguera, R.; Oliveira, T.F. On the design of propeller hydrokinetic turbines: The effect of the number of blades. *J. Braz. Soc. Mech. Sci. Eng.* **2019**, *41*, 253. [CrossRef]
20. Jost, D.; Skerlavaj, A.; Lipej, A. Improvement of efficiency prediction for a kaplan turbine with advanced turbulence models. *Stroj. Vestn.-J. Mech. Eng.* **2014**, *60*, 124–134. [CrossRef]
21. Thake, J. *The Micro-Hydro Pelton Turbine Manual, Design*; ITDG Publishing: Bradford, UK, 2001.
22. Bizzarri, M.; Lavicka, M. Interpolation of Hermite data by clamped Minkowski Pythagorean hodograph B-spline curves. *J. Comput. Appl. Math.* **2021**, *392*, 113469. [CrossRef]
23. Zheng, W.W.; Yu, H.M.; Lu, Z.H. Two-Step Affine Transformation Prediction for Visual Object Tracking. *IEEE Access* **2021**, *9*, 36512–36521. [CrossRef]
24. Wang, X.; Su, J.S. Evaluation of Precision of Custom Edentulous Trays Fabricated with 3D Printing Technologies. *Int. J. Prosthodont.* **2021**, *34*, 109–117. [CrossRef] [PubMed]
25. tanxp. PLM Home NX Surface Video Tutorial. Available online: <http://www.plmhome.com/thread-2426-1-1.html> (accessed on 21 July 2020).